# Central Nervous System

# 13

## Brain Death Angiography Study (Tc-99m-DTPA)

**Overview** The images of the Radionuclide Brain Death Angiography Study depict the regional distribution of blood flow to and the vascular volume in the brain and surrounding structures including the superior sagittal sinus [1].

**Radiopharmaceutical characteristics** The radiopharmaceutical Tc-99m-DTPA is a combination of the ligand diethylenetriaminepentaacetic acid (pentetic acid), a metal chelator, and Tc-99m, a metal. Its chemical structure is shown in Fig. 13.1. The radiopharmaceutical has a molecular weight of 482.31.

**Extraction mechanism** None in the brain. In general, Tc-99m-DTPA readily passes through the capillary endothelium and equilibrates in the extracellular space. However, in the brain it remains in the vascular space except where the blood-brain barrier has been damaged.

**Extraction efficiency** Normally zero.

**Extraction mechanism saturable or non-saturable** Not applicable.

**Interventions** None.

**Imaging** Gamma camera planar imaging with a high-resolution low-energy collimator is the most commonly used.

**Protocol design** The protocol consists of two parts: acquisition of sequential two second images of the brain in the anterior projection for 30 s during the first circulation beginning at the time of injection and acquisition of delayed images of the brain in the anterior projection (Fig. 13.2).

**Quantitative measurements** None.



W.C. Klingensmith III, *The Mathematics and Biology of the Biodistribution of Radiopharmaceuticals-A Clinical Perspective*,
DOI 10.1007/978-3-319-26704-3_13

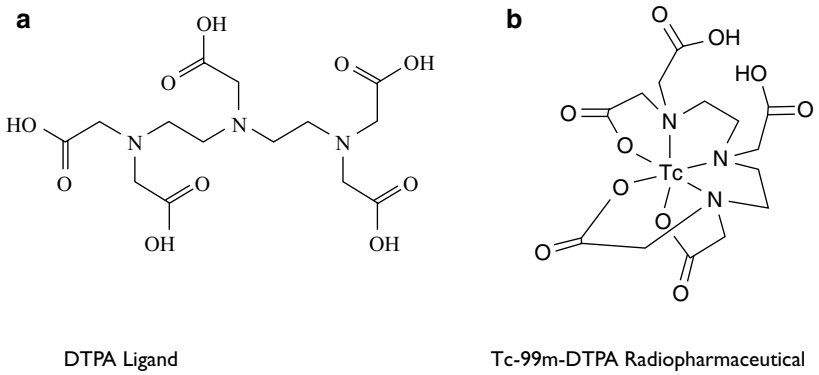


**Fig. 13.1** Chemical diagrams of Tc-99m-DTPA. (**a**) Diethylenetriaminepentaacetic acid (*DTPA*) ligand without the radioisotope Tc-99m. (**b**) Tc-99m-DTPA after the metal chelator, DTPA, has chelated the metal, Tc-99m

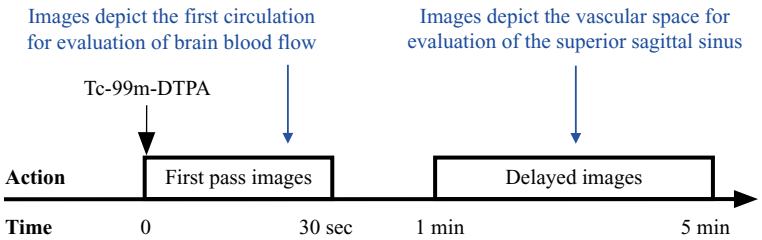


**Fig. 13.2** Protocol summary diagram

## Brain Glucose Metabolism Study (F-18-Fluorodeoxyglucose)

**Overview** The images of the Brain Glucose Metabolism Study with F-18-fluorodeoxyglucose (FDG) depict the distribution of glucose metabolism in the brain in a tomographic fashion. The sole energy source of the brain is glucose, and the gray matter uses three to four times as much glucose as the white matter on a per volume basis [2].

**Radiopharmaceutical characteristics** FDG is an analog of glucose and exists in blood predominantly in the form of soluble FDG. It has a molecular weight of 193.17, and its chemical structure is shown in Fig. 13.3.

**Extraction mechanism** FDG is transported across cell membranes by glucose transporters (GLUTs), which are passive facilitative transporters. Several GLUTs are found in the brain including GLUT1 and GLUT4 (Fig. 13.4) [3].

Once inside the cell, FDG is phosphorylated by the hexokinase enzyme. The addition of a phosphate group to FDG prevents the radiopharmaceutical from diffusing out of the cell. At the same time, the absence of a hydroxyl group at the second carbon position prevents phosphorylated FDG from binding to the next enzyme in the glycolytic pathway. This fact prevents FDG from being metabolized and, in turn, prevents the radiolabel, F-18, from diffusing back out of the cell into the blood (Fig. 13.5).

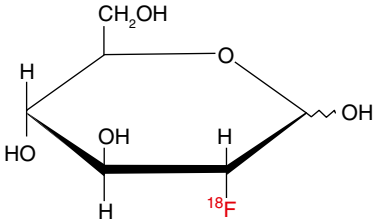


**Fig. 13.3** F-18-Fluorodeoxyglucose (FDG). The hydroxyl group on the second carbon of glucose has been replaced by a positron emitting fluorine-18 atom to form the radiopharmaceutical FDG

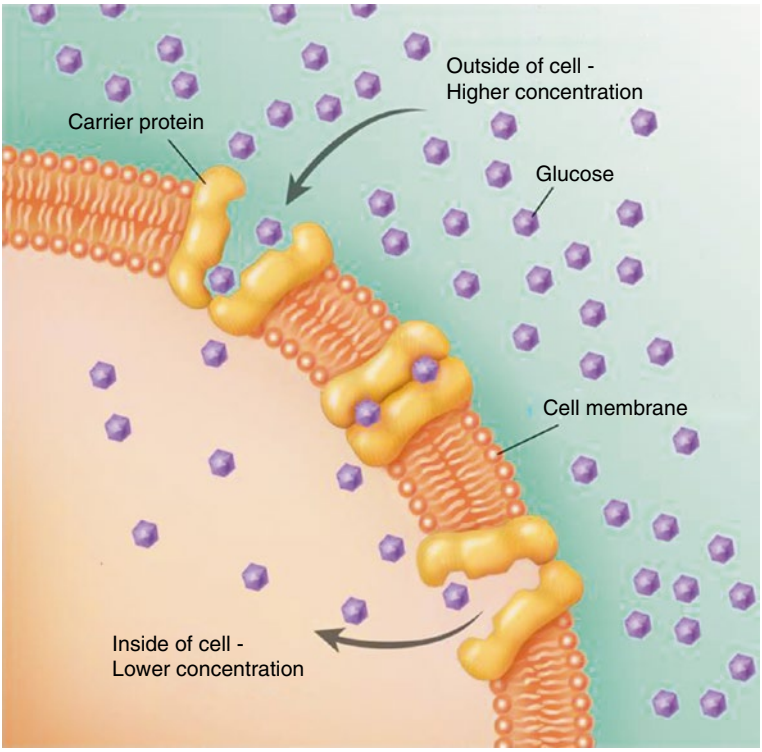


**Fig. 13.4** Transport of glucose across the cell membrane by GLUT1. GLUT transporters are an example of passive facilitative transport which is driven by the concentration gradient of glucose. The gradient is maintained by the intracellular phosphorylation of glucose. When glucose binds to the GLUT transporter, it induces a change in configuration of the transporter which in turn causes the release of the glucose molecule in the intracellular space

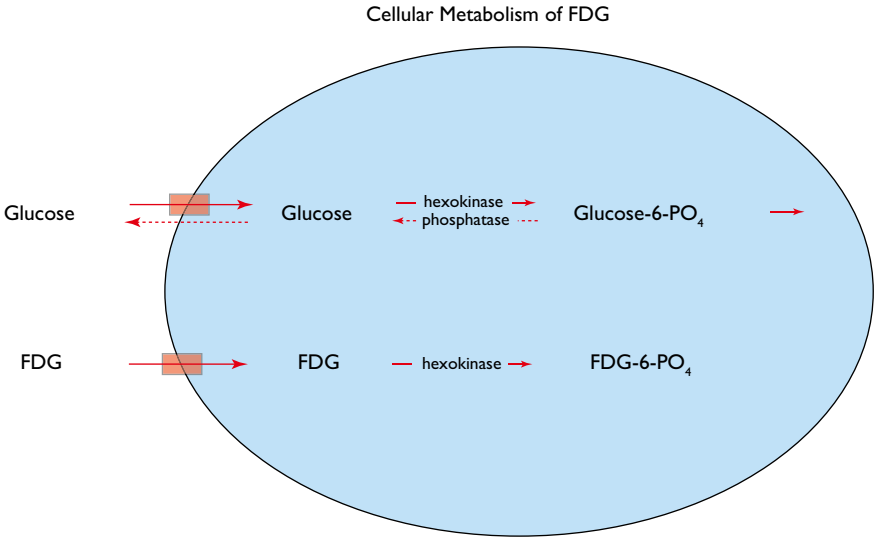


**Fig. 13.5** Cellular uptake of glucose vs. FDG. Most transmembrane glucose transport proteins bind to glucose and FDG equally. In addition, the hexokinase enzyme binds to and phosphorylates glucose and FDG equally well. However, the next enzyme in the glycolytic pathway binds phosphorylated glucose, but not phosphorylated FDG

While differences in the metabolic behavior of FDG compared to native glucose make it an imperfect tracer of glucose, the differences actually improve FDG from an imaging point of view. If F-18 diffused back out of cells, the contrast between cells that clear FDG and background including blood would be decreased. In addition, if FDG were reabsorbed by the kidneys, there would be a greater amount of FDG in the blood and again the contrast between cells that clear FDG and background would be decreased.

**Extraction efficiency** The exact extraction efficiency of FDG in the brain is unknown but is probably higher in gray matter than in white matter [4].

**Extraction mechanism saturable or non-saturable** Saturable. Hyperglycemia increases competition for glucose receptors and decreases clearance of FDG. In addition, hyperglycemia can cause a downregulation of the GLUT receptors so that not only is there an increase in nonradioactive glucose to compete with FDG for GLUT receptors but there are fewer receptors (Fig. 13.6) [5].

**Interventions** None.

**Imaging** F-18 is a positron emitter so imaging is done with a PET-CT scanner. Because the PET images are tomographic, there is no need for background correction. And because the CT images provide high-resolution density maps, the PET images can be corrected for attenuation.

**Protocol design** High-resolution 15 min PET images are obtained beginning at 45 min after administration of the FDG. These glucose metabolism tomograms are compared to the high-resolution CT images of brain anatomy (Fig. 13.7).

**Quantitative measurements** None.

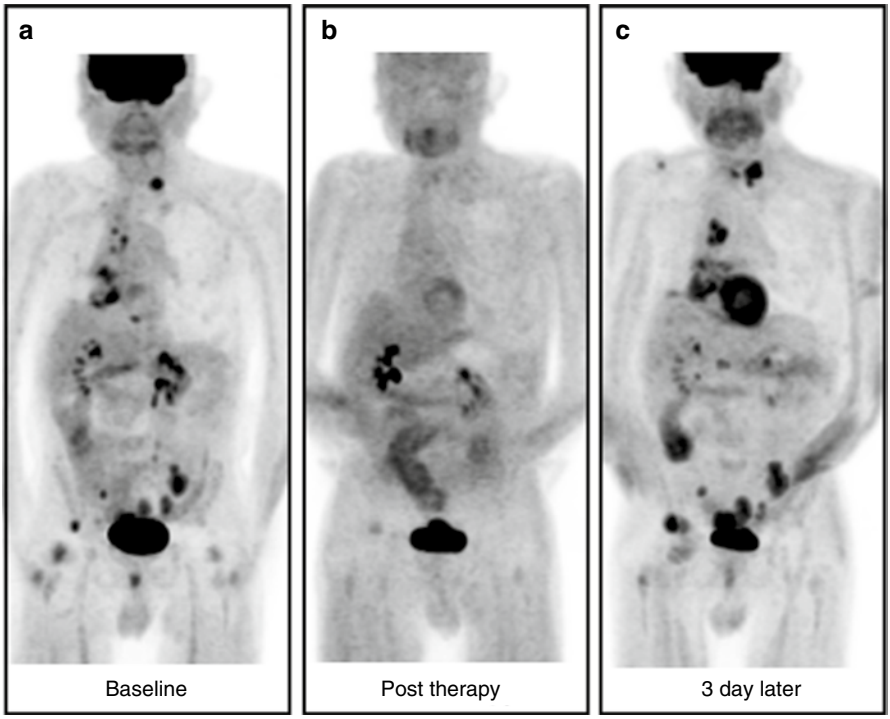


**Fig. 13.6** A 76-year-old male with lung cancer. Anterior MIP (maximum intensity projection) images from sequential FDG PET-CT studies. (**a**) The baseline study shows widespread metastases. The blood glucose was 105 mg/dL. (**b**) Post-therapy (11 weeks later), the metastases appear to have resolved. Of note, there is very little FDG uptake in the brain. The patient was not known to be a diabetic, but the blood glucose was 260 mg/dL. (**c**) The patient was sent to his physician for treatment of newly diagnosed diabetes and the FDG study was repeated 3 days later. At the time of the repeat study, his blood glucose was 76 mg/dL. In comparison to the baseline study, the repeat study demonstrates progressive metastatic disease and normal brain uptake. The elevated blood glucose level at the time of the initial post-therapy study is probably insufficient to fully explain the essentially complete lack of uptake in the metastases and brain. It is postulated that, in addition to a possible competitive effect, the elevated glucose level caused a downregulation of the glucose receptors in tumor and the brain

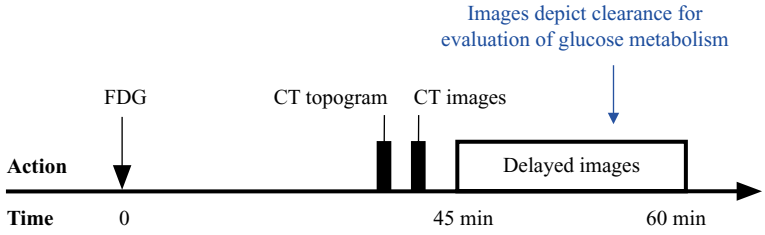


**Fig. 13.7** Protocol summary diagram

## Brain Perfusion Study (Tc-99m-HMPAO)

**Overview** The SPECT images of the Brain Perfusion Study depict the distribution of blood flow and perfusion to the various structures of the brain [6].

However, despite the fact that the title of the study says "brain perfusion," the images actually reflect brain clearance, i.e., primarily blood flow times extraction efficiency. This is true of all nuclear medicine studies that have the word "perfusion" in the title. Relative clearance will reflect relative perfusion or blood flow only as long as the extraction efficiency is uniform throughout the volume that is being imaged, but often it is not.

**Radiopharmaceutical characteristics** Tc-99m-HMPAO (hexamethylpropyleneamineoxime) is a lipophilic molecular complex with a molecular weight of 383.32. Its chemical structure is shown in Fig. 13.8.

**Extraction mechanism** Because of its lipophilic nature, Tc-99m-HMPAO diffuses readily across the endothelial capillaries of the brain, through the blood-brain barrier, and across the cell membranes of neurons (Fig. 13.9). Once in the intracellular space, most of Tc-99m-HMPAO becomes hydrophilic and is unable to diffuse back out of the cell. A small amount binds to intracellular components [8]. At high flow rates, Tc-99m-HMPAO underestimates cerebral blood flow [6].

**Extraction efficiency** The exact extraction efficiency in the brain is unknown but appears to be moderate [6].

**Extraction mechanism saturable or non-saturable** Non-saturable.

**Interventions** None.

**Imaging** Gamma camera SPECT imaging with a high-resolution low-energy collimator and SPECT computer software is the most commonly used.

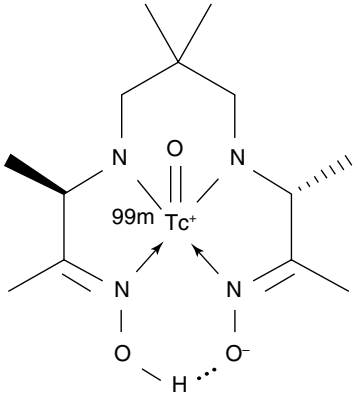


Tc-99m-HMPAO (exametazime)

**Fig. 13.8** Tc-99m-HMPAO (Tc-99m-exametazime)

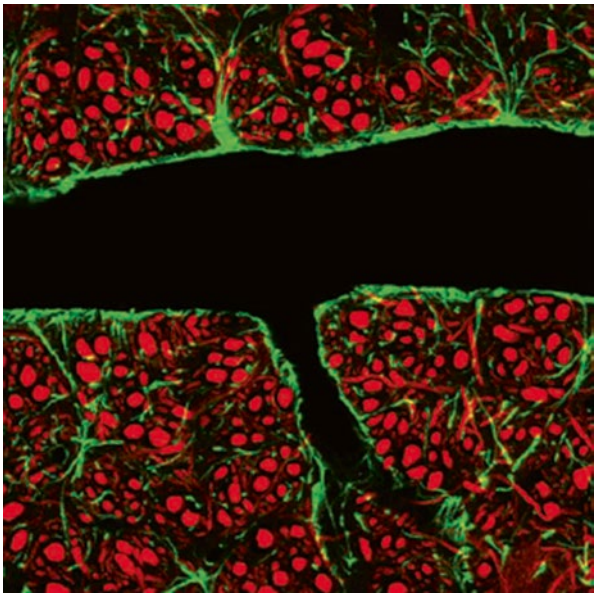

**Fig. 13.9** Blood-brain barrier. The *red* structures represent neurons. The *green* structures are astrocytes that form the blood-brain barrier along the margins of vessel (Emily [7]; original in *Science Translational Medicine*)

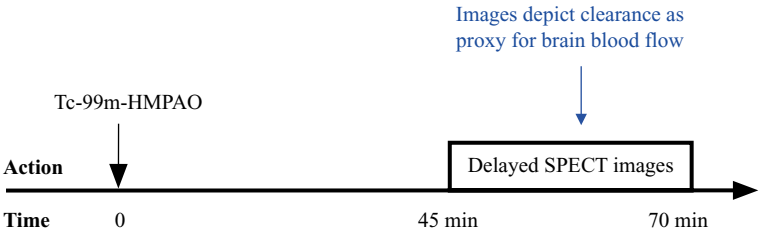


**Fig. 13.10** Protocol summary diagram

**Protocol design** Forty-five minutes after injection of the radiopharmaceutical, SPECT images are acquired of the brain (Fig. 13.10).
**Quantitative measurements** None.

## Cisternography (In-111-DTPA)

**Overview** Cisternography images depict the flow of cerebrospinal fluid along normal and abnormal pathways following injection of the tracer into the lumbar intrathecal space.
**Radiopharmaceutical characteristics** In-111-DTPA is a combination of the ligand diethylenetriaminepentaacetic acid (pentetic acid), a metal chelator, and In-111, a metal. It has a molecular weight of 508.22 D, and its chemical structure is shown in Fig. 13.11.

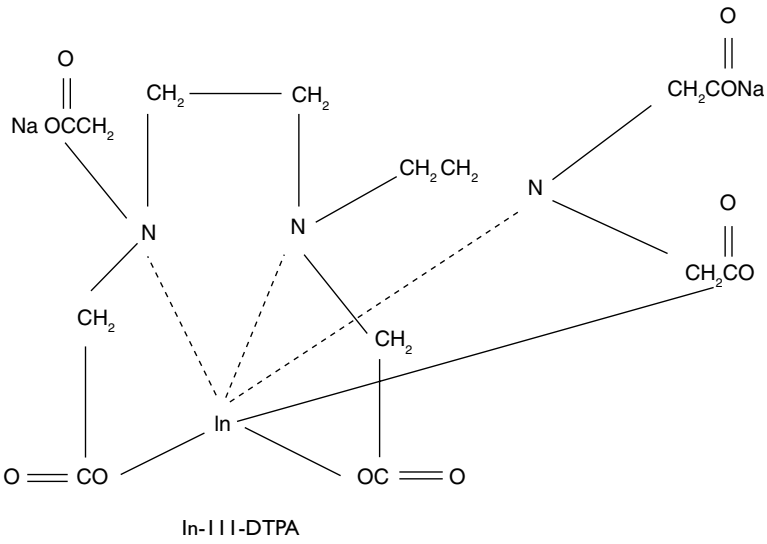


**Fig. 13.11** Chemical structure of In-111-DTPA. Diethylenetriaminepentaacetic acid (DTPA) ligand with the radioisotope In-111

**Extraction mechanism** Until the In-111-DTPA reaches the superior sagittal sinus over the brain, there is no extraction or clearance of the tracer. Once the In-111-DTPA reaches the subarachnoid space over the convexity of the brain, it is reabsorbed along with cerebrospinal fluid (CSF) through the arachnoid villa and into the venous blood of the superior sagittal sinus. Following reabsorption, the tracer is carried away in the venous blood and excreted from the body by glomerular filtration in the kidneys. The exact mechanism by which CSF is reabsorbed by the arachnoid villa is unknown but may involve flow through a one-way valve in the cells of the arachnoid matter [9].

Since In-111-DTPA does not accumulate in the superior sagittal sinus, the images of the head do not directly reflect the reabsorption process, and no extraction mechanism is imaged. During the study, the tracer moves simply with the bulk flow of CSF, and the images demonstrate the pathway and speed of the movement of the tracer through the subarachnoid space from the lumbar region to the top of the brain (Fig. 13.12).

**Extraction efficiency** The extraction efficiency of In-111-DTPA at the arachnoid villa of the superior sagittal sinus is essentially 100 %.

**Extraction mechanism saturable or non-saturable** Non-saturable.

**Interventions** None.

**Imaging** Imaging is performed with a gamma camera fitted with a medium-energy parallel-hole collimator.

**Protocol design** The movement of In-111-DTPA in the CSF after intrathecal injection at the lumbar spine level is imaged over a 24 h period. Delayed images are acquired as needed (Figs. 13.12 and 13.13).

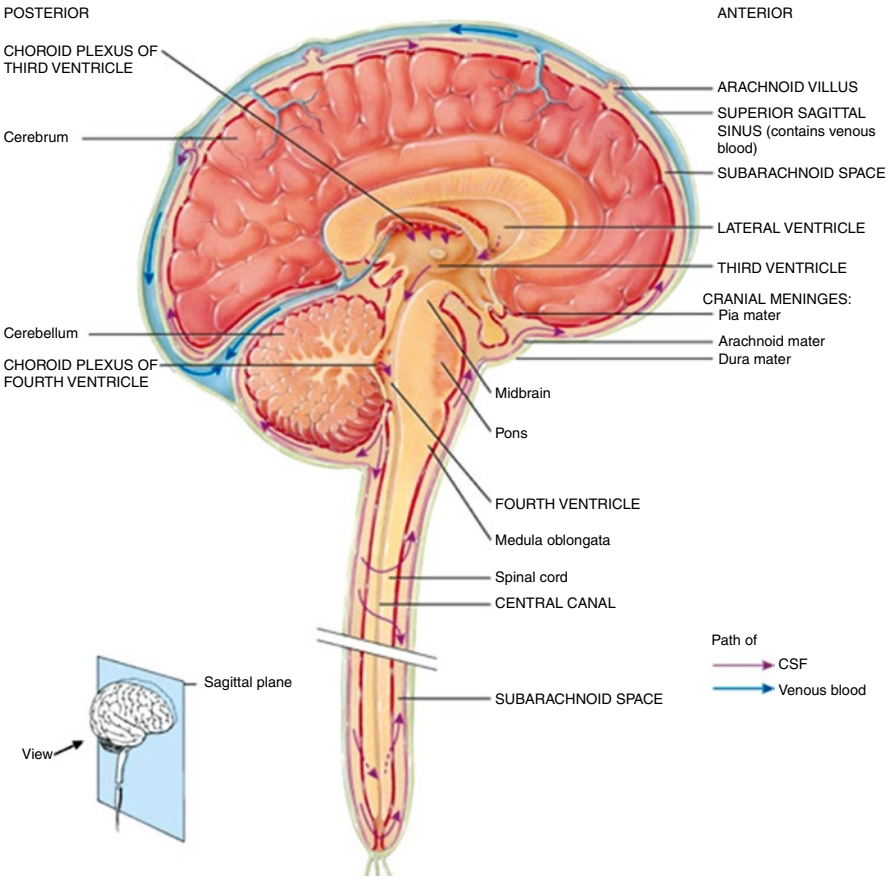


**Fig. 13.12** Sagittal section of brain and spinal cord showing origin, pathway of flow, and site of reabsorption of CSF [10]

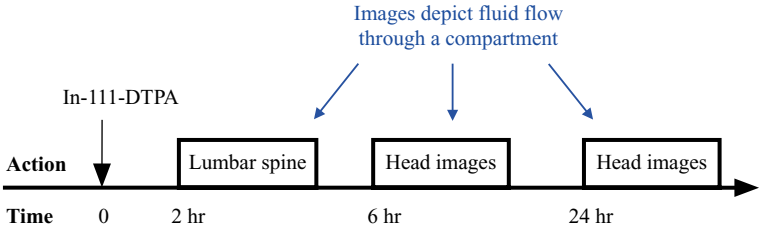


**Fig. 13.13** Protocol summary diagram

**Quantitative measurement** The images essentially reflect the central volume principle (see Chap. 5, Mean Transit Time: Central Volume Principle).

$$\bar{T}\left(\text{sec}\right) = \frac{V\left(\text{mL}\right)}{F\left(\text{mL}/\text{sec}\right)} \sim T_{\text{LE}}\left(\text{sec}\right) \tag{13.1}$$

Here the "central volume principle" equation has been solved for mean transit time instead of flow. $\bar{T}$ represents the mean transit time of blood flow through the subarachnoid space, $V$ represents the volume of the subarachnoid space, $F$ represents the production and flow of CSF, and the symbol "~" stands for "varies as." However, since the subarachnoid space volume and CSF flow cannot be determined, the mean transit time cannot be calculated. Instead, the leading edge transit time, $T_{\text{LE}}$, is assessed visually by noting when the leading edge of the tracer reaches the region of the superior sagittal sinus. Of note, the pathway may change with disease, i.e., reabsorption may occur in the lateral ventricles in addition to or instead of the superior sagittal sinus. The upper limits of normal for the leading edge transit time of the bolus to reach the superior sagittal sinus is 24 hours.

When the cisternogram is performed for the purpose of identifying the source of CSF rhinorrhea, there is also a nonvisual quantitative measurement. Nasal pledgets of a standard size are placed into the anterior and posterior portions of both nasal cavities 2 h after the intrathecal injection of In-111-DTPA and removed 4 h later. In addition, blood samples are drawn at the same two times. The pledget and plasma specimens are counted in a gamma well counter, and the results are expressed as a ratio of the amounts of activity in the pledgets, i.e., nasal cavities, relative to the amount of activity in the plasma.

This measurement represents a quasi-absolute nuclear medicine measurement with plasma activity serving as a proxy for the amount of In-111-DTPA administered intrathecally and pledget activity reflecting the amount of labeled CSF that has leaked into the nasal cavities (see Chap. 10, Other Quantitative Techniques). Any increased activity in the pledgets comes from leakage of CSF containing a relatively high amount of activity from the subarachnoid space at the base of the brain through a break in the dura and skull base to reach the nasal cavity.

**Quantitative measurement: Normal range** The normal range for the pledget to plasma ratio is 1.3 or less [11].

## Striatal Dopamine Transporter Study (I-123-Ioflupane [DaTscan®])

**Overview** The Striatal Dopamine Transporter Study with I-123-ioflupane depicts the prevalence and biodistribution of dopamine transporter receptors at the synaptic junction of the presynaptic neuron in the striatum (putamen and head of the caudate nucleus) [12, 13]. When stimulated by an action potential, i.e., electrical charge, presynaptic storage vesicles filled with dopamine fuse with the presynaptic plasma membrane and release the dopamine into the synaptic cleft. The dopamine molecules transmit a signal by binding to dopamine receptors on the postsynaptic plasma

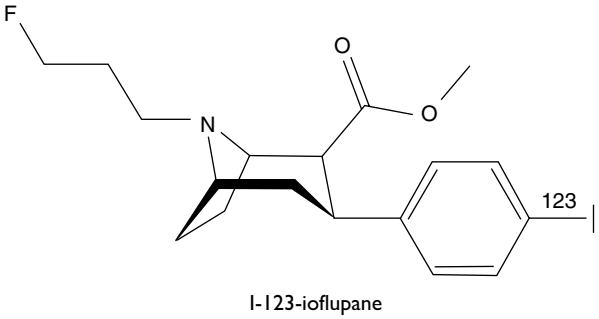


**Fig. 13.14** Chemical structure I-123-ioflupane (DaTscan®)

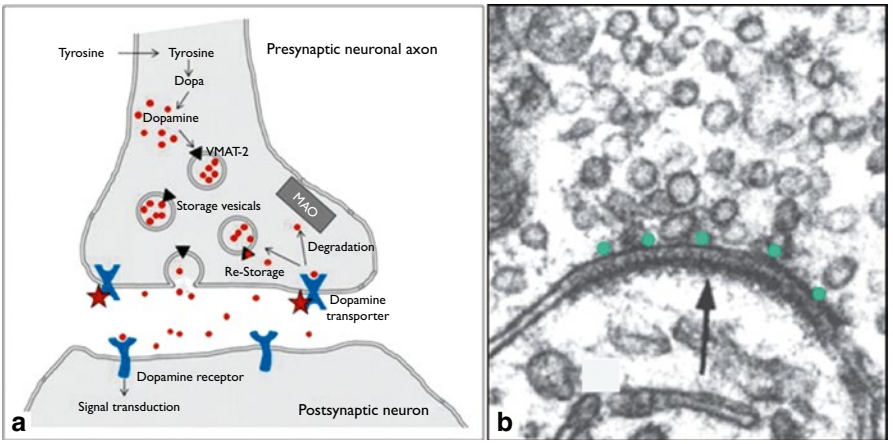


**Fig. 13.15** Neuronal synapse. (**a**) *Red dots* represent dopamine which I-123-ioflupane traces. When an action potential reaches the nerve terminal, dopamine is released, passes across the synapse, and binds to dopamine receptors which initiates a postsynaptic signal. Then free dopamine binds to dopamine transporter receptors on the presynaptic side to be repackaged into vesicles and reused [15]. The *red stars* indicate where I-123-ioflupane binds to the dopamine transporter receptors. (**b**) Electron micrograph shows synaptic junction (*arrow*) with presynaptic axon above (distinguished by numerous vesicles containing neurotransmitters like dopamine) and the postsynaptic axon below with only a few vesicles. The *green dots* represent dopamine transporter proteins in the presynaptic plasma membrane [16]

membrane. The free dopamine molecules bind to dopamine transporters on the presynaptic plasma membrane and are internalized into storage vesicles for reuse [14].

**Radiopharmaceutical characteristics** I-123-ioflupane is derived from cocaine and is a Schedule II controlled substance under the Controlled Substance Act in the USA. Its molecular weight is 289.38 and its chemical structure is shown in Fig. 13.14.

**Extraction mechanism** I-123-ioflupane binds to the dopamine transporter on the presynaptic side of the synaptic junction (Fig. 13.15).

**Extraction efficiency** Unknown.

**Extraction mechanism saturable or non-saturable** Saturable. The drugs of abuse, cocaine and amphetamine, are the ones most likely to decrease the uptake of I-123-ioflupane significantly. These two drugs should be discontinued for 4–5

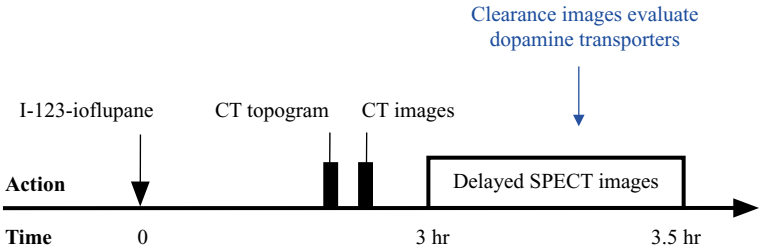


**Fig. 13.16** Protocol summary diagram

plasma clearance half-lives before performing an I-123-ioflupane study [14]. A number of other drug classes and drugs bind to the dopamine transporter with high affinity and may interfere with the Striatal Dopamine Transporter Study [14].
**Interventions** None.
**Imaging** SPECT-CT imaging with a low-energy high-resolution gamma camera collimator and SPECT computer software is the most commonly used.
**Protocol design** SPECT-CT images of the brain are acquired at 3 h after intravenous administration of the radiopharmaceutical (Fig. 13.16).
**Quantitative measurement** None in general.

## Ventricular Shunt Study (Tc-99m-DTPA)

**Overview** The Ventricular Shunt Study evaluates the patency of shunts by direct injection of the radiopharmaceutical into the shunt apparatus.
**Radiopharmaceutical characteristics** Tc-99m-DTPA is a combination of the ligand pentetic acid or diethylenetriaminepentaacetic acid, a metal chelator, and Tc-99m, a metal. Its molecular weight is 482.31 and the chemical structure shown in Fig. 13.1.
**Extraction mechanism** None. The Tc-99m-DTPA is in confined spaces, shunt tubing, and pleural, peritoneal, or vascular spaces.
**Extraction efficiency** Zero.
**Extraction mechanism saturable or non-saturable** Not applicable.
**Interventions** None.
**Imaging** Gamma camera planar imaging with a low-energy high-resolution collimator is the most commonly used.
**Protocol design** Imaging field: Head and shunt pathway; may include neck and chest or neck, chest, and abdomen. Anterior images are usually sufficient. Delayed images may be necessary if activity has not reached the pleura, peritoneum, or vascular space by the end of routine imaging (Fig. 13.17).
**Quantitative measurement** The Tc-99m-DTPA is not injected into the input port to the reservoir chamber but directly into the reservoir (Fig. 13.18).

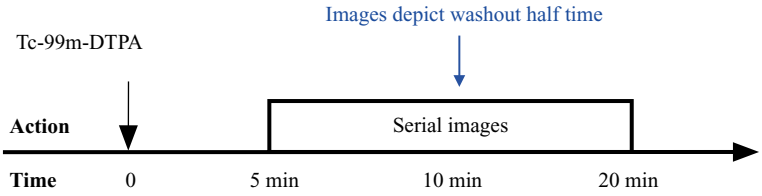


**Fig. 13.17** Protocol summary diagram

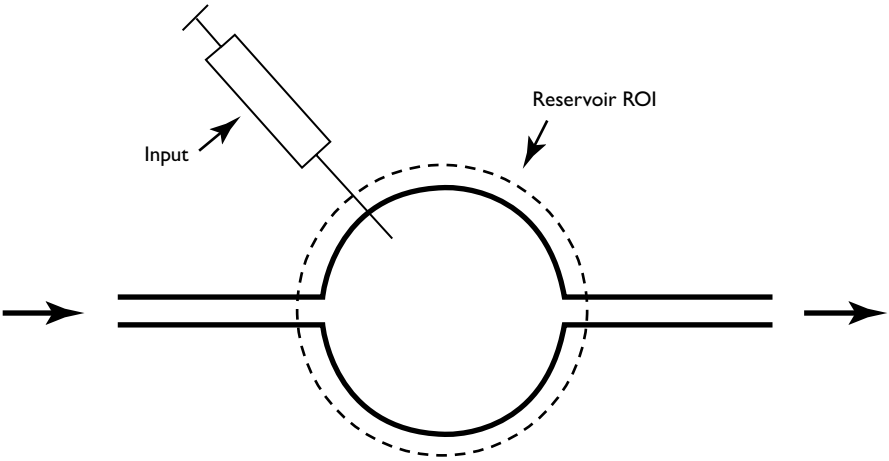


**Fig. 13.18** Single compartment model. The *solid lines* depict a single compartment in the middle, a single input on the left, and a single output on the right. The *broken circle* indicates a region of interest (ROI) for generating a time-activity curve during the first pass of a bolus of activity through the model

Since the reservoir is a small volume and the injection will cause some turbulence in the reservoir, the tracer can be considered to be evenly distributed within the reservoir almost instantaneously. Then the time-activity curve from a ROI over the reservoir will show the residual tracer in the reservoir as a function of time, and the halftime of washout can be calculated.

This measurement is different from the mean transit time through a compartment in which the tracer is injected at the point of inflow, rather than throughout the compartment. The halftime of washout of tracer from a given volume when the tracer is initially uniformly distributed throughout the chamber will be half of the wash time when the tracer is injected at the entry to the chamber, that is, it will be half of the mean transit time (see Chap. 5, Mean Transit Time: Central Volume Principle).

**Quantitative measurement: Normal range** The residual halftime will vary with the make of reservoir because volume of the reservoir varies among manufacturers. These values have been calculated [17–19].

## References

### Brain Death Angiography Study (Tc-99m-DTPA)

1. Zuckier LS, Kolano J. Radionuclide studies in the determination of brain death: criteria, concepts, and controversies. Semin Nucl Med. 2008;38:262–73.

### Brain Glucose Metabolism Study (F-18-Fluorodoxyglucose)

2. Herholz K, Heiss WD. Positron emission tomography in clinical neurology. Mol Imaging Biol. 2004;6:239–69.
3. Wood IS, Trayhurn P. Glucose transporters (GLUT and SGLT): expanded families of sugar transport proteins. Br J Nutr. 2003;89:3–9.
4. Silverman DHS, Melega WP. Molecular imaging of biological processes with PET: evaluating biologic bases of cerebral function. In: Phelps ME, editor. PET: molecular imaging and its biological applications. New York: Springer; 2004. p. 512.
5. Ishizu K, Nishizawa S, Yonekura Y, et al. Effects of hyperglycemia on FDG uptake in human brain and glioma. J Nucl Med. 1994;35:1104–9.

### Brain Perfusion Study (Tc-99m-HMPAO)

6. Payne JK, Trivedi MH, Devous MD. Comparison of technetium-99m-HMPAO and xenon-133 measurements of regional cerebral blood flow by SPECT. J Nucl Med. 1996;37:1735–40.
7. Emily U. Can sound open the brain for therapies? Science. 2015;347:1187.
8. Suess E, Huck S, Reither H, et al. Uptake mechanism of technetium-99m-d, l-HMPAO in cell cultures of the dissociated postnatal rat cerebellum. J Nucl Med. 1992;33:108–14.

### Cisternography (In-111-DTPA)

9. Sakka L, Coll G, Chazal J. Anatomy and physiology of cerebrospinal fluid. Eur Ann Otorhinolaryngol Head Neck Dis. 2011;128:309–16.
10. Cohen BJ. Memmler's the human body in health & disease. Wolters Kluwer Health; 2011.
11. McKusick KA, Malmud LS, Kordela PA, et al. Radionuclide cisternography: normal values for nasal secretion of intrathecally injected in-111-DTPA. J Nucl Med. 1973;14:933–4.

### Striatal Dopamine Transporter Study (I-123-Ioflupane)

12. Djang DSW, Jansen MJR, Bhenen N, et al. SNM practice guideline for dopamine transporter imaging with I-123-ioflupane SPECT 1.0. J Nucl Med. 2012;53:154–63.
13. Membrane transport of small molecules and the electrical properties of the cell. In: Albert B, Johnson A, Lewis J, Raff M, Roberts K, Walter P, editors. Molecular biology of the cell. 5th ed. New York: Garland Science; 2008. p 808.

14. Booij J, Kemp P. Dopamine transporter imaging with I-123-FP-CIT SPECT: potential effects of drugs. Eur J Nucl Med. 2008;35:424–38.
15. Djang DSW, Jansen MJR, Bhenen N, et al. SNM practice guideline for dopamine transporter imaging with I-123-ioflupane SPECT 1.0. J Nucl Med. 2012;53:154–63.
16. Mescher AL. Junqueira's Basic histology text & atlas. New York: McGraw Hill Lange; 2013. p. 166.

## Ventricular Shunt Study (Tc-99m-DTPA)

17. Harbert J, Haddad D, McCullough D. Quantitation of cerebrospinal fluid shunt flow. J Nucl Med. 1974;112:379–87.
18. Chervu S, Chervu LR, Vallabhajosyula B, et al. Quantitative evaluation of cerebrospinal fluid shunt flow. J Nucl Med. 1984;25:91–5.
19. Harbert JC, McCullough DC. Radionuclide tests of cerebral fluid shunt patency. J Nucl Med. 1984;25:112–4.